Supporting Information for *Resolution Enhancement of Flood Inundation Grids*

Bryant Seth[1,2], Schumann Guy[3], Apel Heiko[1], Kreibich Heidi[1], and Merz Bruno[1,2]

[1]GFZ German Research Centre for Geosciences, Section 4.4. Hydrology, Potsdam, Germany
[2]Institute of Environmental Science and Geography, University of Potsdam, Potsdam, Germany
[3]School of Geographical Sciences, University of Bristol, Bristol, TN, UK

Correspondence: Seth Bryant (seth.bryant@gfz-potsdam.de)

S1 Resample Case

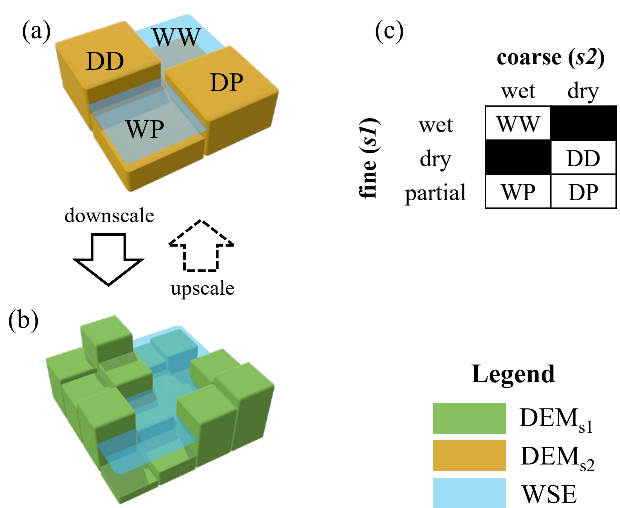

Figure S1. Framework for classification of flood hazard resample case. Panel (a) shows conceptual coarse grids and the corresponding resample case calculated from Eq. 1. Panel (b) shows the corresponding fine grids while Panel (c) shows the case label acronyms. D, W, and P stand for *dry*, *wet*, and *partial*, respectively.

S2 Case Study

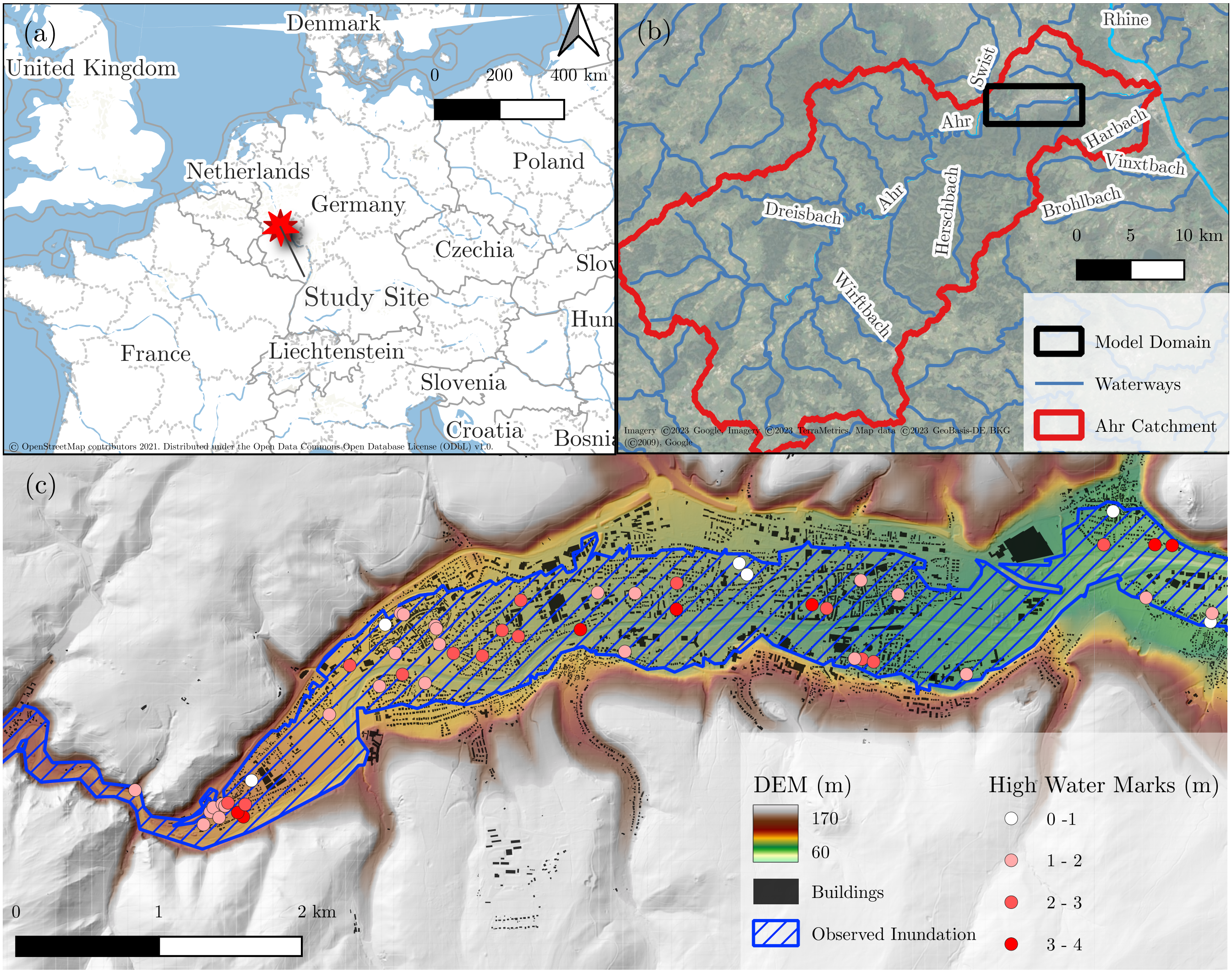

Figure S2. Study site maps showing: (a) location map; (b) Ahr catchment map; and (c) downscaling domain with main datasets (see Table S1 for descriptions).

Table S1. Summary of data used

type	metadata	ref.
DEM	0.5 m resolution bare earth DEM created from aerial LiDAR survey from September 22 to October 24, 2021 in twelve sessions with a RIEGL scanner LMS-VQ780i with 20 points/m^2 achieved.	(Milan Geoservice GmbH, 2023)
High water marks	75 high water marks at buildings reported by residents.	(Apel et al., 2022)
Inflow hydrograph	30 hour hydrograph at Altenahr gauge with maximum depth of 10.2 m reconstructed by Environmental Office of the federal state Rhineland-Palatinate.	(Apel et al., 2022)
Building locations	Building footprint polygons downloaded from OSM on 2022-11-14.	(OpenStreetMap contributors, 2022)
Observed inundation	Polygon of maximum flood extents compiled from an aerial survey on July 16th and 20th and a second survey on July 24th and 29th.	(Landesamt für Umwelt Rheinland-Pfalz, 2022)
Land cover	Gridded land cover inventory reflecting 2017-2018 conditions and updated in 2020.	(Copernicus Land Monitoring Service, 2018)

S3 Inundation Performance Metrics

Quantitative evaluation of flood inundation grids is commonly accomplished using a diverse set of metrics that communicate and quantify over- and under-predictions and their proportions. To compute these metrics, simulations for maximum inundation are evaluated against some observed binary data grid of wet and dry cells. First, each cell is classified according to Table S2 by comparing the simulated to the observed data grids to generate a confusion map. From this confusion map, the total counts of each of the four classifications is computed. These total counts are then used to calculate the domain-wide inundation metrics commonly used in flood inundation evaluation shown in Table S3.

Table S2. Inundation confusion matrix. For a given simulation, each cell in the domain is compared to the corresponding cell in the observed grid and classified according to this table. Adapted from Wing et al. (2017).

		Simulated	
		Wet	Dry
Observed	Wet	True Positive (TP)	False Negative (FN)
	Dry	False Positive (FP)	True Negative (TN)

Table S3. Flood inundation performance metrics. See Table S2 for acronyms. Adapted from Wing et al. (2017).

Metric	Equation	Poor	Perfect	Description
Critical Success Index	$\frac{TP}{TP+FP+FN}$	0	1	ratio of accurate wet cells to total wet cells and missed wet cells
Hit Rate	$\frac{TP}{TP+FN}$	0	1	portion of observed wet cells reproduced by the model
False Alarms	$\frac{FP}{TP+FP}$	1	0	portion of modelled wet cells which are erroneous
Error Bias	$\frac{FP}{FN}$	0 or inf	1	ratio of over-predictions to under-predictions

S4 Hydrodynamic Model Calibration

To obtain accurate water level grids at coarse ($s2 = 32m$) and fine ($s1 = 4m$) resolutions, twin hydrodynamic models are constructed in the RIM2D platform and calibrated using a mix of brute force and scipy's implementation of the Newton-Conjugate Gradient algorithm (Nocedal and Wright, 2006; Virtanen et al., 2020). Roughness values for built-up and channel/floodplain are treated as two (independent) free parameters for the optimization. A single performance metric, Critical Success Index (CSI) defined in Table S3, is calculated against the observed inundation for each iteration and used to optimize with the free parameters. Optimization trials were undertaken on a Tesla P100 GPU using python scripts.

Results of the two calibration trials are shown in Fig. S3 and S4. The performance metrics shown in Table S3 are also shown; however, only CSI was used for optimization. In general, the fine ($s1 = 4m$) model replicates the target inundation with over- and under-predictions roughly balancing (Error Bias = 1.2) while the coarse model ($s2 = 32m$) generally under-predicts when CSI is optimized (Error Bias = 0.33). Focusing on water surface elevations (which were not part of the optimization), the fine ($s1 = 4m$) model has lower WSE values upstream and higher WSE values downstream when compared to the coarse ($s2 = 32m$); likely owing to the difficulties in modelling the narrower channel in this region at the coarser resolutions. Note the performance metrics reported in the manuscript are computed on a smaller domain.

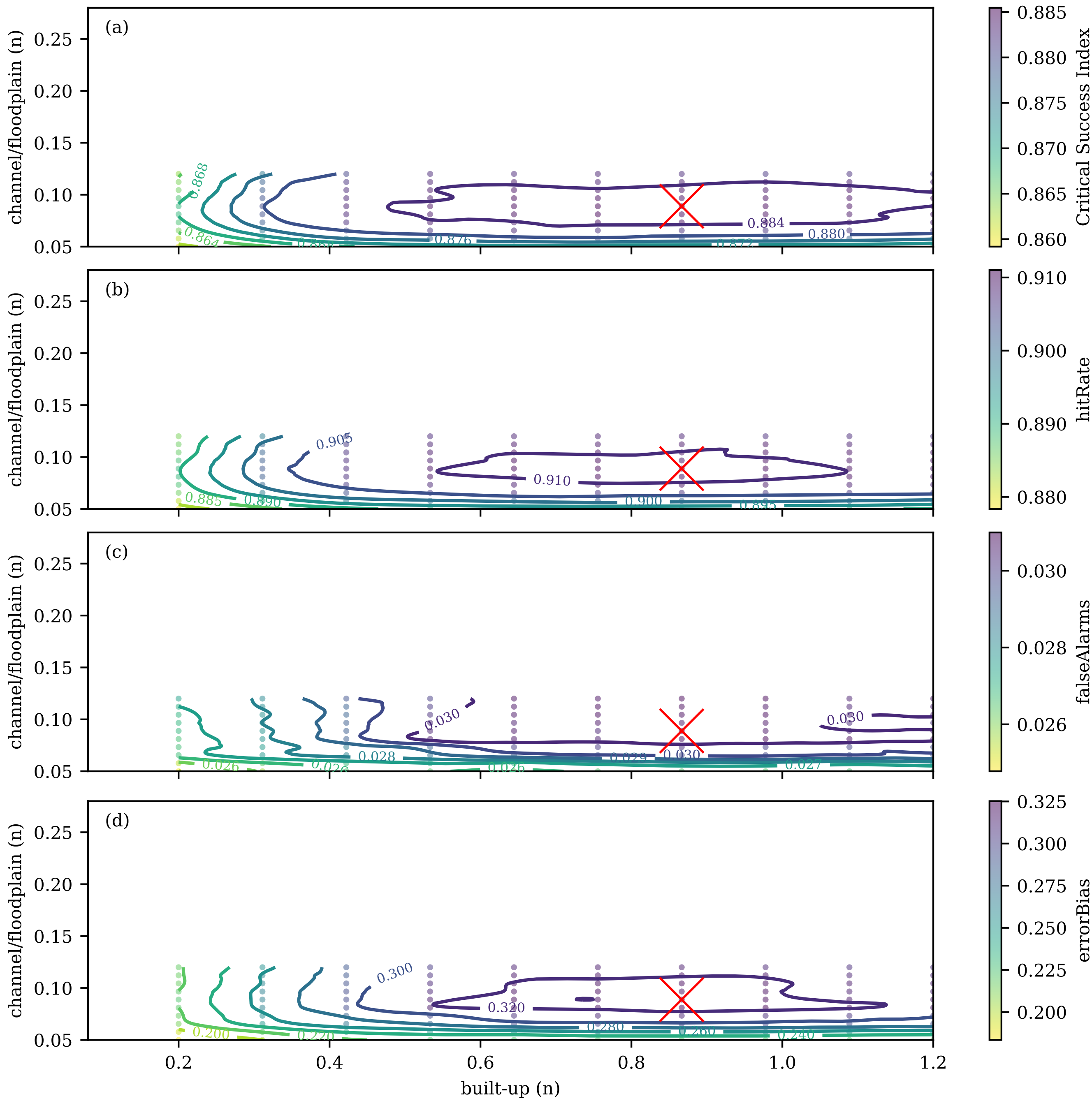

Figure S3. Calibration results for 32 m hydrodynamic model showing the four metrics from Table S3. Points denote individual model runs (at the shown roughness) and contours are computed via interpolation of the metric value at each point. Red 'X' marks the optimal (using the maximum CSI) and the parameterization used for downscaling.

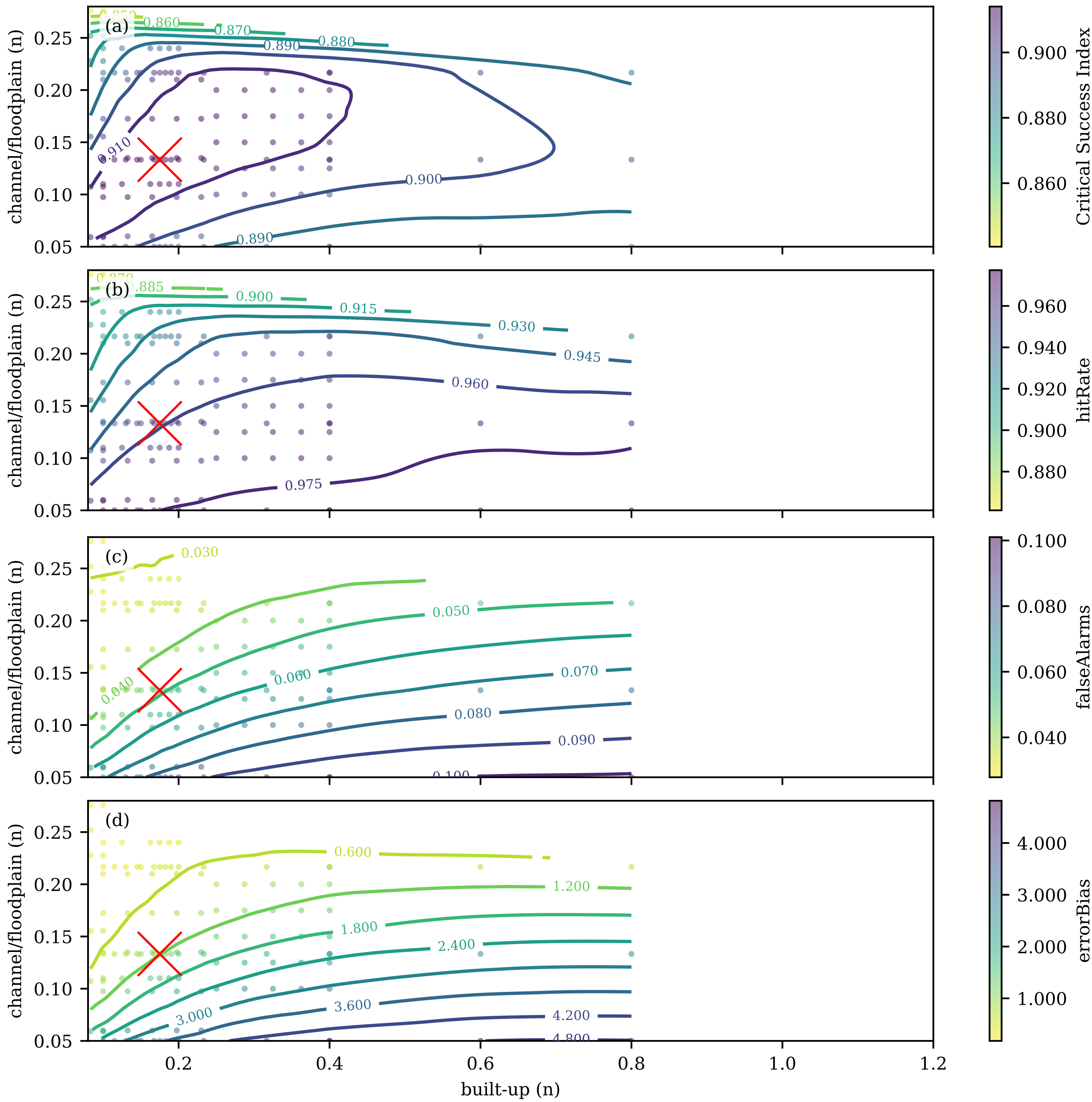

Figure S4. Calibration results for 4 m hydrodynamic model similar to Figure S3.

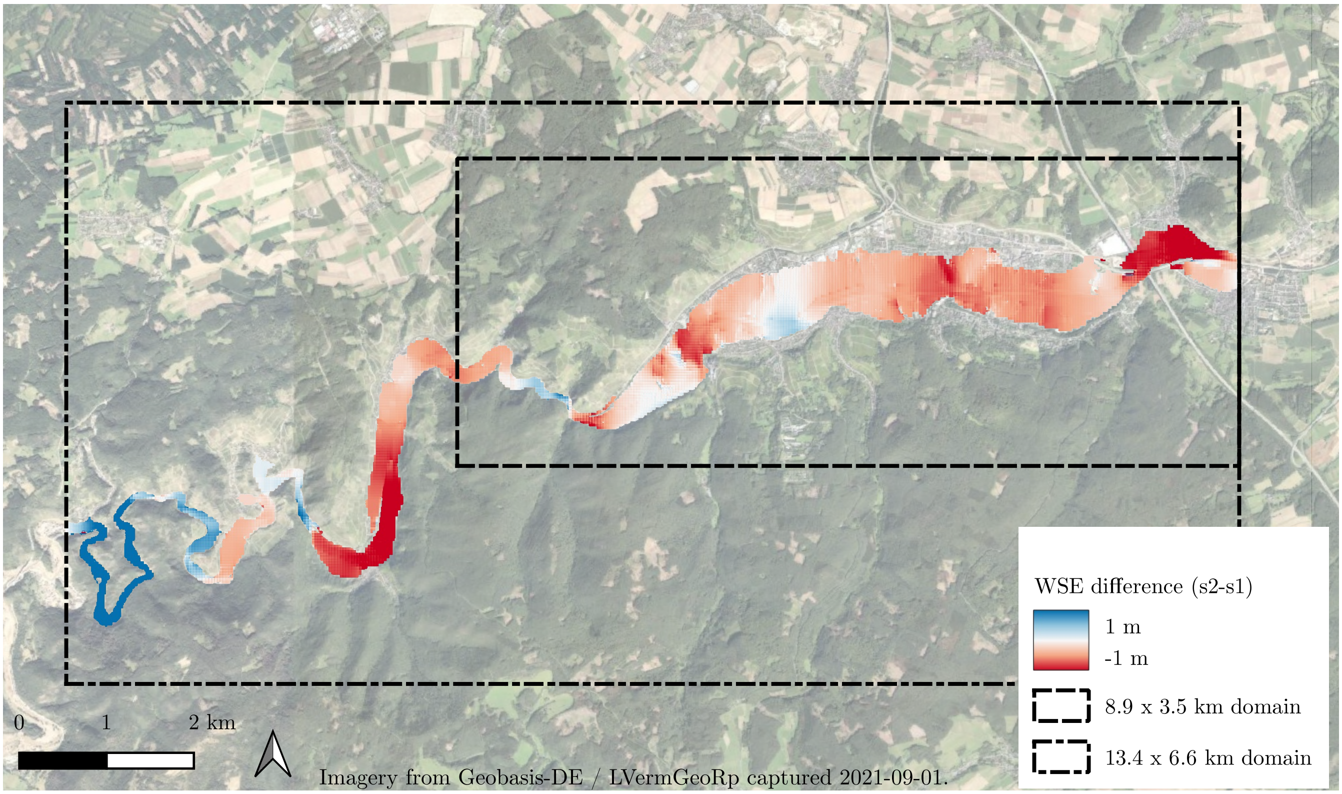

Figure S5. WSE max difference between coarse ($s2 = 32m$) and fine ($s1 = 4m$) models at their respective optimum roughnesses clipped to intersecting inundation region. Red denotes regions where the fine ($s1 = 4m$) solution yielded higher or larger water depths than the coarse ($s2 = 32m$). Domain used for hydrodynamic modelling (13.4 x 6.6 km) and subset used for downscaling analysis (8.9 x 3.5 km) shown in black for reference.

References

Apel, H., Vorogushyn, S., and Merz, B.: Brief communication: Impact forecasting could substantially improve the emergency management of deadly floods: case study July 2021 floods in Germany, Natural Hazards and Earth System Sciences, 22, 3005–3014, https://doi.org/10.5194/nhess-22-3005-2022, 2022.

Copernicus Land Monitoring Service: European Union, Copernicus Land Monitoring Service 2018, European Environment Agency (EEA), https://land.copernicus.eu/pan-european/corine-land-cover, 2018.

Landesamt für Umwelt Rheinland-Pfalz: Hochwasser im Juli 2021, Tech. rep., Landesamt für Umwelt Rheinland-Pfalz, https://lfu.rlp.de/fileadmin/lfu/Wasserwirtschaft/Ahr-Katastrophe/Hochwasser_im_Juli2021.pdf, 2022.

Milan Geoservice GmbH: Airborne Laser Scanning (ALS) Ahr Valley, Tech. Rep. D-01917 Kamenz, 2023.

Nocedal, J. and Wright, S. J.: Numerical Optimization, Springer Series in Operations Research and Financial Engineering, Springer New York, https://doi.org/10.1007/978-0-387-40065-5, 2006.

OpenStreetMap contributors: Planet dump retrieved from https://planet.osm.org, published: https://www.openstreetmap.org, 2022.

Virtanen, P., Gommers, R., Oliphant, T. E., Haberland, M., and Contributors), R. S. .: SciPy 1.0: Fundamental Algorithms for Scientific Computing in Python, Nature Methods, 17, 261–272, https://doi.org/10.1038/s41592-019-0686-2, 2020.

Wing, O. E. J., Bates, P. D., Sampson, C. C., Smith, A. M., Johnson, K. A., and Erickson, T. A.: Validation of a 30 m resolution flood hazard model of the conterminous United States: 30 m RESOLUTION FLOOD MODEL OF CONUS, Water Resources Research, 53, 7968–7986, https://doi.org/10.1002/2017WR020917, 2017.